PHILOSOPHICAL TRANSACTIONS OF THE ROYAL SOCIETY A MATHEMATICAL, PHYSICAL & ENGINEERING SCIENCES

Stick-Slip Motion of Turbine Blade Dampers

F. Pfeiffer and M. Hajek

Phil. Trans. R. Soc. Lond. A 1992 **338**, 503-517
doi: 10.1098/rsta.1992.0017

Stick–slip motion of turbine blade dampers

By F. Pfeiffer[1] and M. Hajek[2]

[1] *Department of Mechanical Engineering, Technical University of München, Germany*
[2] *Messerschmitt–Bölkow–Blohm, Helicopter Division, Ottobrunn, Germany*

Turbine blade dampers are small elements of a parabolic configuration usually fabricated from sheet steel. They are positioned loosely between the roots of turbine blades improving the damping of blade vibrations by generating dry friction from the relative motion of blades and damper. This paper presents a theoretical approach to these stick–slip vibrations and compares theory with measurements. Additionally, some design aspects of such dampers are discussed by considering the damping behaviour in relation to important design parameters.

1. Introduction

Turbine blades in gas-turbines are components subjected to extremely high loads with respect to force and temperature. They are excited by pressure fluctuations in the hot gas-stream mainly with frequencies that are whole multiples of the rotor angular frequency. Because of an extreme centrifugal force field there is practically no relative motion between the blade roots and the turbine disc and, additionally, structural damping is very small. Therefore, damping devices are used; these are located between the blade platforms and pressed into this gap by centrifugal forces. The blade vibrations induce relative motion between dampers and blade platforms leading to dry friction and thus to a damping effect. The main problem connected with the operation of such damper devices consists of the centrifugal forces, which can press these dampers into the gap in such a way that there is only static but no sliding friction and consequently no damping. Therefore, damper design must follow the requirement to produce as much sliding friction as possible and to minimize static friction situations. This can be achieved by proper design of the damper form, which usually is parabolic or circular, and by an appropriate choice of damper parameters like mass and contact angles.

Proper design of that kind cannot be done by systematic experiments, which would be too expensive. Therefore, we develop in the following a planar model of a turbine blade damper which allows some design parameter variations. The model consists of two blades, each one represented by two masses only and of the damper in a parabolic or circular form. The damper possesses two points of contact, where the parabola or circle of the damper meets the straight line of the blade platform. In these contact points we may have stiction, slippage or rolling without sliding. The possibility of rolling with sliding is not considered. The mathematical model for this configuration will be a patching method putting together the solutions of the various sets of equations of motion that are valid from one friction event to another.

The literature on frictional vibrations is large, the references give a small selection with some emphasis on turbine damping problems. Some principal early works are

Phil. Trans. R. Soc. Lond. A (1992) **338**, 503–517
Printed in Great Britain

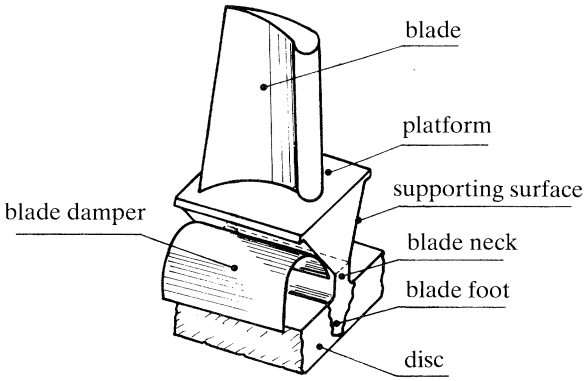

Figure 1. Typical blade configuration.

connected with names like den Hartog (1931), Klotter (1938), Reissig (1954), Magnus (1976) and Kato (1974). The problem of den Hartog has been reconsidered by Marui (1984). All these contributions illustrate the well-known fact that analytic solutions for dry friction problems can only be achieved for very simple systems. Some newer considerations on the general problems of frictional behaviour may be found in Guckenheimer (1983), Schiehlen (1983) and Shaw (1986), where, in particular, Guckenheimer (1983) applies modern mathematical methods of nonlinear dynamics and topological mechanics to the problem. Authors like Panagiotopoulos (1985), Moreau (1985*a*, *b*, 1988) and Lötstedt (1981, 1982, 1979) take quite a different approach by applying new methods of convex analysis to stick–slip problems, which results in better mechanical definiteness and less numerical difficulties. Some typical contributions to the problem of turbine blade damping are given by Beards (1985), Goodman (1956), Griffin (1981), Hundal (1979), Jones (1978, 1979), Lalanne (1985), Ramamurti (1984), Rao (1980) and Sinha (1983).

At the Technical Institute of Munich stick–slip and impulsive processes have been the matter subject of research for many years. Pfeiffer (1984) presents a starting point and Pfeiffer (1991) gives an overview. Hajek (1990) is the main basis of this contribution and the work of Brandl (1988) contains some general remarks on dry friction, whereas Brandl *et al.* (1987) present a fundamental theory on an order-n-algorithm for multibody systems.

2. Modelling

2.1. *Mechanical model*

Figure 1 shows a typical configuration of a turbine blade with platform and blade root, which is connected with the disc. The blade damper is usually located between the supporting surfaces of two adjoining blades. If we have a certain number of blades, n, around a disc there is the same number of blade dampers. We may assume that all blade dampers contact the supporting surfaces along a straight line.

With n blades and dampers we then have $2n$ contact lines, where stick–slip processes take place. Theoretical formulation of such a large frictional system involves no problems in general, but a numerical realization would probably run aground due to excessive computing times. Therefore, the model is simplified further. We consider only a planar mechanical model with two blades and one damper and thus with two points of contact, which should be sufficient to evaluate parameter

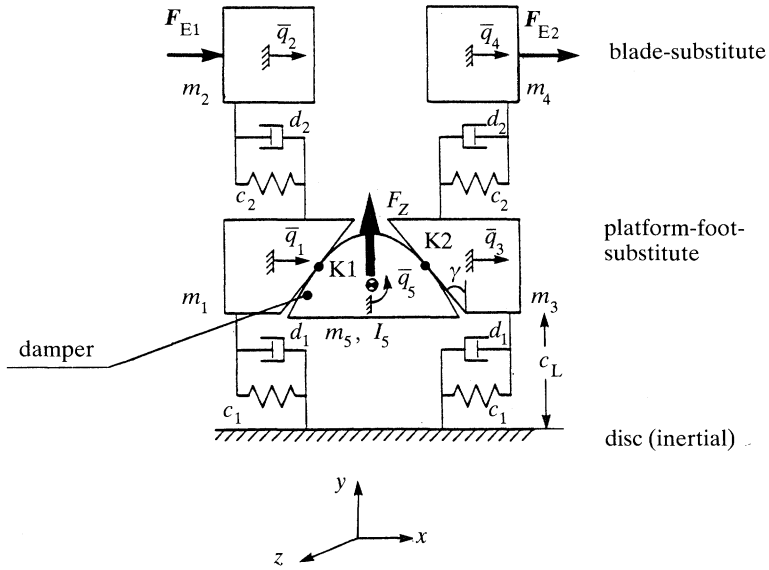

Figure 2. Mechanical model of blade damper configuration.

tendencies. Further, we restrict the model to the lower eigenfrequencies of the blade, which makes some sense due to a practical experience that these lower shares of the spectrum have most influence on the damper motion. These assumptions and simplifications lead to a mechanical model as shown in figure 2.

Each of the two blades is substituted by two masses and by two spring–dashpot systems. The contour of the damper, the locations of contact points and the inclination angle of the supporting surface are modelled with the real turbine data. The magnitudes of the two blade masses and of the spring–dashpot combination are determined by a corresponding modal reduction of FEM-calculations. The system is excited by gas-stream fluctuation forces represented in the model by the forces $\boldsymbol{F}_{E1}$ and $\boldsymbol{F}_{E2}$, which are known from the gas-turbine aerodynamics.

The mechanical model possesses five degrees of freedom in the case of sliding friction on both contact points. If one of the contact points starts a transition to static friction one degree of freedom is lost, and we are left with four degrees of freedom. In the case of static friction in both contact points only three degrees of freedom are left. In any case of static friction this situation always means rolling without sliding because the blades continue to vibrate thus generating movements of the contact points. We shall exclude a separation of the dampers from the supporting surfaces, because it will be unlikely within the existing very large centrifugal force field.

From this the following combination of degrees of freedom are possible (figure 2):

sliding K1, K2, $\boldsymbol{q}^{\mathrm{T}} = (q_1, q_2, q_3, q_4, q_5)$, (1)

sliding K1, stiction K2, $\boldsymbol{q}^{\mathrm{T}} = (q_1, q_2, q_3, q_4)$, (2)

stiction K1, sliding K2, $\boldsymbol{q}^{\mathrm{T}} = (q_1, q_2, q_3, q_4)$, (3)

stiction K1, K2, $\boldsymbol{q}^{\mathrm{T}} = (q_1, q_2, q_4)$. (4)

The damper mass possesses only one rotational degree of freedom, all blade masses have translational degrees of freedom.

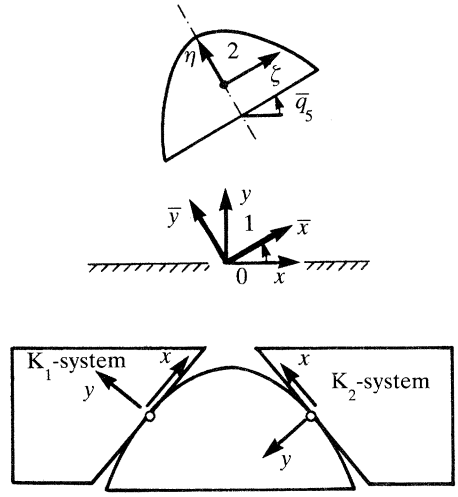

Figure 3. Coordinate systems for the damper and its contact points.

2.2. *Geometry and constraints*

Although the model of figure 2 looks quite simple, the geometry in the points of contact and therefore the kinematical properties will be complicated. In a first step we consider coordinate systems.

For most kinematical relations and for the equations of motion we use an inertially fixed xy system (index '0' in figure 3). For convenience it is sometimes better to have the system '1' of identical origin as system '0' but rotating with the damper angular velocity $\dot{q}_5$. The $\xi\eta$ coordinate system '2' is a body-fixed frame of the damper especially well suited for contact geometry. The same is true for the systems K1, K2 fixed in the blade platforms.

The main aim of the geometrical considerations consists in evaluating the closed loop conditions for the four possible movements, sliding in both contacts, sliding in one contact only and stiction in both contacts. For any of these modes we have the two closing conditions (figure 4)

$$\Delta \boldsymbol{r}_1 = \boldsymbol{r}_{\mathrm{K1}} - \boldsymbol{r}_1 - \boldsymbol{r}_{\mathrm{S}} = 0, \tag{5}$$

$$\Delta \boldsymbol{r}_2 = \boldsymbol{r}_{\mathrm{K2}} - \boldsymbol{r}_2 - \boldsymbol{r}_{\mathrm{S}} = 0, \tag{6}$$

with

$$ {}_0\boldsymbol{r}_{\mathrm{K}i} = \begin{pmatrix} x_{\mathrm{K}i} \\ y_{\mathrm{K}i} \\ 0 \end{pmatrix}, \quad {}_2\boldsymbol{r}_i = \begin{pmatrix} \xi_i \\ \eta_i \\ 0 \end{pmatrix}, \quad {}_0\boldsymbol{r}_i = \begin{pmatrix} x_i \\ y_i \\ 0 \end{pmatrix}, \quad {}_0\boldsymbol{r}_{\mathrm{S}} = \begin{pmatrix} x_{\mathrm{S}} \\ y_{\mathrm{S}} \\ 0 \end{pmatrix}, \quad (i = 1, 2). \tag{7}$$

The left index signifies the corresponding coordinate frame. The transformation matrix from base 2 to base 0 is simply

$$A_{02} = \begin{pmatrix} \cos q_5 & -\sin q_5 & 0 \\ \sin q_5 & \cos q_5 & 0 \\ 0 & 0 & 1 \end{pmatrix}. \tag{8}$$

The equations (5), (6) are four scalar equations for six unknowns. We get two additional equations by the requirement that

$$(\mathrm{d}\eta/\mathrm{d}\xi)_{\mathrm{parabola}} = (\mathrm{d}\eta/\mathrm{d}\xi)_{\mathrm{straight\,line}} \tag{9}$$

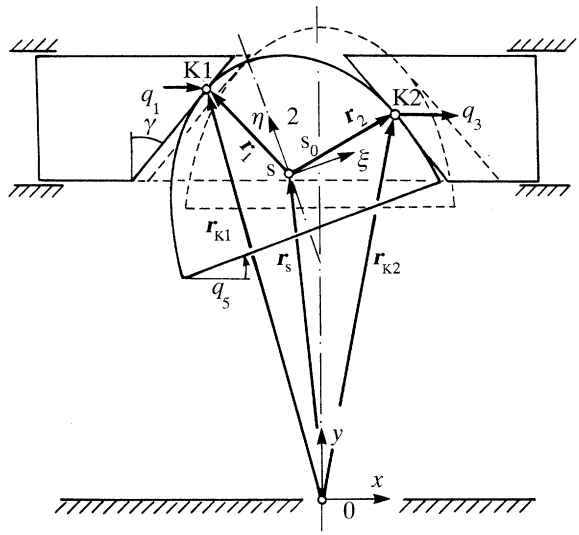

Figure 4. Contact geometry of damper and platforms.

for each of the contact points K1, K2. With the equations (5), (6) and (9) we have now six scalar equations for the unknowns $(x_{K1}, x_{K2}, \xi_1, \xi_2, x_S, y_S)$. It is convenient to evaluate (5) and (6) in the coordinate frame '0' and (9) in the base '2'. The closing equations have to be supplemented by the contour equations for the parabola and the two straight lines, which write

$$\text{parabola (base 2)}, \quad \eta = p_1 \xi^2 + p_2, \tag{10}$$

$$\text{straight line (base 0)}, \quad y_{Ki} = a_i x_{Ki} + b_i(\boldsymbol{q}) \quad (i = 1, 2), \tag{11}$$

where, according to figure 4, $p_1 < 0$ and $p_2 > 0$. The coefficients of (11) follow directly from figure 4:

$$\left.\begin{aligned} a_1 &= \cot\gamma, \quad a_2 = -\cot\gamma, \quad b_1 = b_0 + y_{S0} - q_1 \cot\gamma, \\ b_2 &= b_0 + y_{S0} + q_3 \cot\gamma, \quad b_0 = p_2 - (\cot\gamma)/2p_1. \end{aligned}\right\} \tag{12}$$

The magnitudes b_{10} and y_{S0} are those for the undisturbed reference configuration ($|{}_0\boldsymbol{r}_{S0}| = y_{S0}$ in (7)). Equations (5)–(11) always yield a uniquely defined solution for the unknowns $(\xi_1, \xi_2, x_{K1}, x_{K2}, x_S, y_S)$ dependent on the generalized coordinates $\boldsymbol{q}$; that is

$$\xi_1 = +\frac{\cot(\gamma + q_5)}{2p_1}, \quad \xi_2 = -\frac{\cot(\gamma - q_5)}{2p_1}, \tag{13}$$

$$\left.\begin{aligned} x_{K1} &= \tfrac{1}{2}(q_1 + q_3) + \frac{\sin^2\gamma \cos\gamma}{2p_1 \sin^2(\gamma + q_5) \sin(\gamma - q_5)}, \\ x_{K2} &= \tfrac{1}{2}(q_1 + q_3) - \frac{\sin^2\gamma \cos\gamma}{2p_1 \sin(\gamma + q_5) \sin^2(\gamma - q_5)}, \end{aligned}\right\} \tag{14}$$

$$\left.\begin{aligned} x_S &= x_{K1} - \xi_1 \cos q_5 + (p_1 \xi_1^2 + p_2) \sin q_5, \\ y_S &= (a_1 x_{K1} + b_1) - \xi_1 \sin q_5 - (p_1 \xi_1^2 + p_2) \cos q_5. \end{aligned}\right\} \tag{15}$$

These equations may be linearized with respect to the generalized coordinate q_5. The

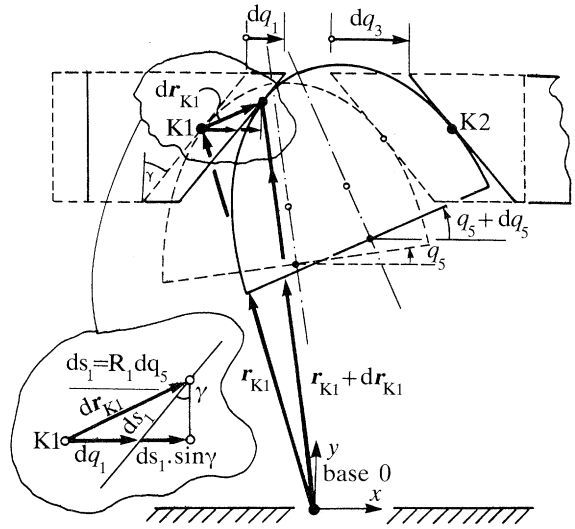

Figure 5. Rolling without sliding in one point.

derivation of the velocities and the accelerations from the holonomic–scleronomic constraints (13)–(15) is straightforward, although it might be advisable to perform the following developments by application of a formula manipulator (Hajek 1990).

With equations (13)–(15) we know the constraint for a motion with sliding in K1, K2 (equation (1)). The second important case is sliding in one point and rolling without sliding in the second point (equations (2), (3)). From figure 5 we see that a differential change of the vector $(\boldsymbol{r}_{K1})$ to $(\boldsymbol{r}_{K1}+\mathrm{d}\boldsymbol{r}_{K1})$ can be decomposed into two parts. The first part is the differential change $(\mathrm{d}q_1)$ of the coordinate q_1, and the second part is a differential contribution due to rolling. From this we get

$$ {}_0(\boldsymbol{r}_{K1}+\mathrm{d}\boldsymbol{r}_{K1})-{}_0(\boldsymbol{r}_{K1})=\begin{pmatrix}\mathrm{d}q_1\\0\\0\end{pmatrix}+\begin{pmatrix}\sin\gamma\\\cos\gamma\\0\end{pmatrix}\mathrm{d}s_1, \tag{16}$$

where $(\mathrm{d}s_1)$ easily follows from the straight line equation (11)

$$ \mathrm{d}s_1=\sqrt{(1+(y'_{K1})^2)}\,\mathrm{d}x_{K1}. \tag{17}$$

On the other hand the differential $(\mathrm{d}x_{K1})$ is not free, but constrained by rolling with the local radius of curvature $R_1=1/\kappa_1$

$$ \mathrm{d}s_1=R_1\cdot\mathrm{d}q_5=\mathrm{d}q_5/\kappa_1, \tag{18}$$

$$ \kappa_1=\eta''/[1+(\eta')^2]^{\frac{3}{2}}. \tag{19}$$

Similar arguments hold, of course, for rolling without sliding in point K2. Combining the equations (14), (16), (17), (18), (19) and the comparable equations for K2 we come out with an additional constraint for the configuration rolling without sliding in one point (equations (2), (3)) in the linearized form

$$ \Delta\dot{q}_1=\dot{q}_5-p_1(\dot{q}_1-\dot{q}_3)=0,\quad \text{for K1}, \tag{20}$$

$$ \Delta\dot{q}_2=\dot{q}_5+p_1(\dot{q}_1-\dot{q}_3)=0,\quad \text{for K2}. \tag{21}$$

The nonlinear form (in q_5) again may be derived by applying a formula manipulator system (Hajek 1990).

In the last case of rolling without sliding on both contact points the damper sticks between the two masses m_1 and m_3 (figures 2, 5) and no rotation q_5 occurs. The masses m_1, m_3, m_5 move as one mass. Therefore, the constraints are simply

$$\dot{q}_1 = \dot{q}_3 = \dot{x}_S, \quad \dot{q}_5 = 0. \tag{22}$$

2.3. *Relative kinematics*

The absolute velocities of the damper and the blade bases (degrees of freedom q_1, q_3, figure 2) can be derived from above expressions. For the two contact points on the damper side we get

$$(\boldsymbol{v}_{Ki})_D = \begin{pmatrix} \dot{x}_S \\ \dot{y}_S \\ 0 \end{pmatrix} + \begin{pmatrix} 0 \\ 0 \\ \dot{q}_5 \end{pmatrix} \times \begin{pmatrix} x_i \\ y_i \\ 0 \end{pmatrix} \quad (i = 1, 2). \tag{23}$$

The blade supporting surfaces move at the same points with

$$(\boldsymbol{v}_{K1})_B = \begin{pmatrix} \dot{q}_1 \\ 0 \\ 0 \end{pmatrix}, \quad (\boldsymbol{v}_{K2})_B = \begin{pmatrix} \dot{q}_3 \\ 0 \\ 0 \end{pmatrix}. \tag{24}$$

The difference of blade and damper velocities must be projected into the direction of the supporting surfaces, which results in the following expressions for the four cases (1)–(4):

sliding K1, K2:

$$\left.\begin{aligned} v_{rel1} &= \dot{q}_1 \frac{1}{2\sin\gamma} + \dot{q}_3 \frac{1}{2\sin\gamma} + \dot{q}_5 \frac{-\cos\gamma(y_1-y_2)+\sin\gamma(x_1-x_2)}{2\sin\gamma\cos\gamma}, \\ v_{rel2} &= \dot{q}_1 \frac{1}{2\sin\gamma} + \dot{q}_3 \frac{1}{2\sin\gamma} + \dot{q}_5 \frac{-\cos\gamma(y_1-y_2)-\sin\gamma(x_1-x_2)}{2\sin\gamma\cos\gamma}, \end{aligned}\right\} \tag{25}$$

sliding K1, stiction K2:

$$\left.\begin{aligned} v_{rel1} &= \dot{q}_1 \frac{(x_1-x_2)}{\cos\gamma(y_1-y_2)+\sin\gamma(x_1-x_2)} + \dot{q}_3 \frac{(x_1-x_2)}{\cos\gamma(y_1-y_2)+\sin\gamma(x_1-x_2)}, \\ v_{rel2} &= 0, \end{aligned}\right\} \tag{26}$$

stiction K1, sliding K2:

$$\left.\begin{aligned} v_{rel1} &= 0, \\ v_{rel2} &= \dot{q}_1 \frac{(x_1-x_2)}{\cos\gamma(y_1-y_2)-\sin\gamma(x_1-x_2)} + \dot{q}_3 \frac{(x_1-x_2)}{\cos\gamma(y_1-y_2)-\sin\gamma(x_1-x_2)}, \end{aligned}\right\} \tag{27}$$

stiction K1, K2:

$$v_{rel1} = 0, \quad v_{rel2} = 0. \tag{28}$$

These are again nonlinear equations. For convenience and with regard to the computer program the terms with (x_1-x_2) and (y_1-y_2) have not been expressed explicitly by (q_1, q_2, q_5) (see (11) and (14)).

2.4. *Dynamics*

The constraints as discussed in §2.2 produce constraint forces which appear as normal or tangential contact forces in the two contact points depending on the type of motion (equations (1)–(4)). For the free motion type with five degrees of freedom ($\boldsymbol{q} \in \mathbb{R}^5$) we can formally write down seven equations of motion, six momentum equations for the four masses and the damper and one moment of momentum equation for the damper (figure 2). In addition to the five unknown accelerations $\ddot{q}_i\,(i = 1, \ldots, 5)$ we have two unknown normal forces in the contact point. If we eliminate from the momentum equations for the damper the accelerations $(\ddot{x}_S, \ddot{y}_S)$ with the help of the constraints (15), (13), (14), we are left with exactly seven equations for seven unknowns.

Similarly, if rolling in one point is going to happen, we get an additional constraint force in tangential direction at the point of contact, which might be determined by replacing $(q_5, \dot{q}_5, \ddot{q}_5)$ in the equations of motion with the help of one of the constraints (20), (21) and thus determining the unknown constraint force. The same procedure will be applied to static friction in both contact points. To put it more formally, we start with the equations of motion in the form

$$\boldsymbol{M}\ddot{\boldsymbol{q}} = \boldsymbol{h}(\boldsymbol{q}, \dot{\boldsymbol{q}}, t) \tag{29}$$

with (figures 2 and 4)

$$\left.\begin{aligned} \boldsymbol{q}^{\mathrm{T}} &= (q_1, q_2, q_3, q_4, q_5, x_S, y_S) \in \mathbb{R}^7, \\ \boldsymbol{M} &= \mathrm{diag}\,(m_1, m_2, m_3, m_4, I_5, m_5, m_5) \in \mathbb{R}^{7,7}, \\ \boldsymbol{h} &\in \mathbb{R}^7, \end{aligned}\right\} \tag{30}$$

$\boldsymbol{q}$ is the vector of generalized coordinates, $\boldsymbol{M}$ the symmetric mass matrix, and the vector $\boldsymbol{h}$ contains all forces in the system.

The two contact constraints (15) may be written as

$$\left.\begin{aligned} d_1(\boldsymbol{q}) &= x_S - [x_{K1} - \xi_1 \cos q_5 + (p_1 \xi_1^2 + p_2) \sin q_5] = 0, \\ d_2(\boldsymbol{q}) &= y_S - [(a x_{K1} + b_1) - \xi_1 \sin q_5 - (p_1 \xi_1^2 + p_2) \cos q_5] = 0. \end{aligned}\right\} \tag{31}$$

For combining (29) and (31) it is convenient to derive the constraints (31) twice

$$d_i(\boldsymbol{q}) = 0, \quad (\partial d_i / \partial \boldsymbol{q})\,\dot{\boldsymbol{q}} = 0, \quad \left(\frac{\partial d_i}{\partial \boldsymbol{q}}\right)\ddot{\boldsymbol{q}} + \frac{\partial}{\partial \boldsymbol{q}}\left(\frac{\partial d_i}{\partial \boldsymbol{q}}\dot{\boldsymbol{q}}\right)\dot{\boldsymbol{q}} = 0, \tag{32}$$

which is abbreviated by the expression

$$\boldsymbol{w}_i^{\mathrm{T}}(\boldsymbol{q})\,\ddot{\boldsymbol{q}} + w_{0i}(\boldsymbol{q}, \dot{\boldsymbol{q}}) = 0 \quad (i = 1, 2). \tag{33}$$

These closing conditions generate normal constraint forces $\boldsymbol{\lambda}^{\mathrm{T}} = (\lambda_1, \lambda_2)$, which must be known to determine the sliding friction forces

$$\boldsymbol{F}_{\mathrm{T}i} = -\mu_S |\boldsymbol{F}_{\mathrm{N}i}|\,(\boldsymbol{v}_{\mathrm{rel},i} / |\boldsymbol{v}_{\mathrm{rel},i}|) \in \mathbb{R}^3 \tag{34}$$

($i = 1, 2$; μ_S = sliding friction coefficient, $\boldsymbol{F}_{\mathrm{T}i}$ = sliding friction forces, $\boldsymbol{F}_{\mathrm{N}i}$ = normal forces, $\boldsymbol{v}_{\mathrm{rel},i}$ = relative velocities, §2.3). The normal forces possess the direction of the surface normal $\boldsymbol{n}_i$ (perpendicular to the supporting plane in figure 1), that is $\boldsymbol{F}_{\mathrm{N}i} = \lambda_i \boldsymbol{n}_i$ and $|\boldsymbol{F}_{\mathrm{N}i}| = \lambda_i$. Care must be taken in combining the equations (29), (33), (34) by introducing lagrangian multipliers $\boldsymbol{\lambda}$, which are defined in the configuration

PHILOSOPHICAL TRANSACTIONS OF THE ROYAL SOCIETY A MATHEMATICAL, PHYSICAL & ENGINEERING SCIENCES

space ($\boldsymbol{q} \in \mathbb{R}^f$) with ($f = 7$), whereas $\boldsymbol{F}_{\mathrm{T}i} \in \mathbb{R}^3$ is defined in a workspace. Therefore, we must transform $\boldsymbol{F}_{\mathrm{T}i}$ by

$$\boldsymbol{F}^*_{\mathrm{T}i} = \left(\frac{\partial \boldsymbol{r}_{\mathrm{K}i}}{\partial \boldsymbol{q}}\right)^{\mathrm{T}} \boldsymbol{F}_{\mathrm{T}i} = \boldsymbol{J}^{\mathrm{T}}_{\mathrm{T}i} \boldsymbol{F}_{\mathrm{T}i} = -\mu_{\mathrm{S}} \boldsymbol{J}^{\mathrm{T}}_{\mathrm{T}i} \left(\frac{\boldsymbol{v}_{\mathrm{rel},\,i}}{|\boldsymbol{v}_{\mathrm{rel},\,i}|}\right) \lambda_i = -\boldsymbol{w}_{\mathrm{S}i}\, \lambda_i, \tag{35}$$

where the $\boldsymbol{r}_{\mathrm{K}i}$ are known from the equations (5), (6), (13), (14) and (15).

Equations (29), (33) and (34) describe the case of sliding friction in two points of contact. If we have stiction in one point, the additional constraints (20) and (21) must be considered; again these can be represented in an acceleration form

$$\boldsymbol{w}^{\mathrm{T}}_{\mathrm{St},\,i}\, \ddot{\boldsymbol{q}} + w_{\mathrm{St0},\,i}(\boldsymbol{q}, \dot{\boldsymbol{q}}) = 0 \quad (i = 1, 2), \tag{36}$$

where in the linearized case $w_{\mathrm{St0},\,i} = 0$. Therefore, for any combination of sliding friction and stiction we can summarize the above relations in the following way by applying a lagrangian multiplier approach

$$\left.\begin{aligned} &\boldsymbol{M}\ddot{\boldsymbol{q}} + \boldsymbol{W}_{\mathrm{St}}\, \boldsymbol{\lambda}_{\mathrm{S}} + (\boldsymbol{W} + \boldsymbol{W}_{\mathrm{S}})\, \boldsymbol{\lambda} - \boldsymbol{h} = 0, \\ &\boldsymbol{W}^{\mathrm{T}}_{\mathrm{St}}\, \ddot{\boldsymbol{q}} + \boldsymbol{W}_{\mathrm{S0}} = 0, \quad \boldsymbol{W}^{\mathrm{T}} \ddot{\boldsymbol{q}} + \boldsymbol{W}_0 = 0, \end{aligned}\right\} \tag{37}$$

with the matrices and vectors

$$\left.\begin{aligned} \boldsymbol{W}_{\mathrm{St}} &= (\ldots\ldots\ \boldsymbol{w}_{\mathrm{St},\,z_j}\ \ldots\ldots) && \text{with} \quad (z_j \in n_{\mathrm{a}}), \\ \boldsymbol{W} &= (\ldots\ldots\ \boldsymbol{w}_{z_i}\ \ldots\ldots) && \text{with} \quad (z_i \in (2 - n_{\mathrm{a}})), \\ \boldsymbol{W}_{\mathrm{S}} &= (\ldots\ldots\ \boldsymbol{w}_{\mathrm{S},\,z_i}\ \ldots\ldots) && \text{with} \quad (z_i \in (2 - n_{\mathrm{a}})), \\ \boldsymbol{W}_{\mathrm{S0}} &= (\ldots\ldots\ w_{\mathrm{St0},\,z_j}\ \ldots\ldots)^{\mathrm{T}} && \text{with} \quad (z_j \in n_{\mathrm{a}}), \\ \boldsymbol{W}_0 &= (\ldots\ldots\ w_{0z_i}\ \ldots\ldots)^{\mathrm{T}} && \text{with} \quad (z_i \in (2 - n_{\mathrm{a}})). \end{aligned}\right\} \tag{38}$$

The magnitude n_{a} is the number of active constraints ($n_{\mathrm{a}} \leqslant 2$). The index scheme (z_j, z_i) defines the changing combination of constraints just being active. The matrix $\boldsymbol{W}_{\mathrm{St}} \in \mathbb{R}^{7,\,2n_{\mathrm{a}}}$ represents the static friction case as given above with $(2n_{\mathrm{a}})$ active constraints, the matrix $\boldsymbol{W} \in \mathbb{R}^{7,\,(2-n_{\mathrm{a}})}$ represents the sliding friction case with $(2 - n_{\mathrm{a}})$ active constraints. The matrix $\boldsymbol{W}_{\mathrm{S}} \in \mathbb{R}^{7,\,(2-n_{\mathrm{a}})}$ summarizes the sliding friction forces as given with (35), and the vectors $\boldsymbol{W}_{\mathrm{S0}} \in \mathbb{R}^{2n_{\mathrm{a}}}$ and $\boldsymbol{W}_0 \in \mathbb{R}^{2-n_{\mathrm{a}}}$ put together the $w_{\mathrm{S}0i}$ – and w_{0i} – terms of the equations (36) and (33). According to the discussion above the vector $\boldsymbol{\lambda}_{\mathrm{S}} \in \mathbb{R}^{2n_{\mathrm{a}}}$ are static friction constraint forces and $\boldsymbol{\lambda} \in \mathbb{R}^{2-n_{\mathrm{a}}}$ are sliding friction constraint forces.

The equations (37) represent $(7 + 2n_{\mathrm{a}} + (2 - n_{\mathrm{a}}))$ scalar equations for the same number of unknown accelerations $\ddot{\boldsymbol{q}}$ and forces $\boldsymbol{\lambda}_{\mathrm{S}}$ and $\boldsymbol{\lambda}$. They can be solved for the unknowns preferably in two steps, with regard to the fact that the constraint equations are always decoupled from constraint forces $\boldsymbol{\lambda}_{\mathrm{S}}, \boldsymbol{\lambda}$. Therefore, putting $\ddot{\boldsymbol{q}}$ from the first equation (37) into the second and third equations we obtain for $\boldsymbol{\lambda}_{\mathrm{S}}, \boldsymbol{\lambda}$ the following set:

$$\begin{bmatrix} (\boldsymbol{W}^{\mathrm{T}}_{\mathrm{St}} \boldsymbol{M}^{-1} \boldsymbol{W}_{\mathrm{St}})\ (\boldsymbol{W}^{\mathrm{T}}_{\mathrm{St}} \boldsymbol{M}^{-1} (\boldsymbol{W} + \boldsymbol{W}_{\mathrm{S}})) \\ (\boldsymbol{W}^{\mathrm{T}} \boldsymbol{M}^{-1} \boldsymbol{W}_{\mathrm{St}})\ (\boldsymbol{W}^{\mathrm{T}} \boldsymbol{M}^{-1} (\boldsymbol{W} + \boldsymbol{W}_{\mathrm{S}})) \end{bmatrix} \begin{bmatrix} \boldsymbol{\lambda}_{\mathrm{S}} \\ \boldsymbol{\lambda} \end{bmatrix} = \begin{bmatrix} \boldsymbol{W}^{\mathrm{T}}_{\mathrm{St}} \boldsymbol{M}^{-1} \boldsymbol{h} + \boldsymbol{W}_{\mathrm{S0}} \\ \boldsymbol{W}^{\mathrm{T}} \boldsymbol{M}^{-1} \boldsymbol{h} + \boldsymbol{W}_0 \end{bmatrix}. \tag{39}$$

Knowing $\boldsymbol{\lambda}_{\mathrm{S}}$ and $\boldsymbol{\lambda}$ we can compute $\ddot{\boldsymbol{q}}$ from

$$\ddot{\boldsymbol{q}} = \boldsymbol{M}^{-1}[-\boldsymbol{W}_{\mathrm{St}}\, \boldsymbol{\lambda}_{\mathrm{S}} - (\boldsymbol{W} + \boldsymbol{W}_{\mathrm{S}})\, \boldsymbol{\lambda} + \boldsymbol{h}]. \tag{40}$$

This set of equations generates automatically the correct combination of magnitudes $\ddot{\boldsymbol{q}}, \boldsymbol{\lambda}_{\mathrm{S}}, \boldsymbol{\lambda}$, which corresponds to the combination of active constraints and thus to the

actual degrees of freedom. This statement is true if existence and definiteness of the solution is assured, which can be shown for special cases. Critical configurations are always bodies with more than one stick–slip contact. General aspects of this problem are still a matter of on-going research.

2.5. *Switching conditions*

The transition from sliding friction to static friction is indicated by vanishing relative velocity $v_{\mathrm{rel},i}(\boldsymbol{q},\dot{\boldsymbol{q}})=0$, and it is secured if the static friction force $\mu_{\mathrm{S}i}|\boldsymbol{F}_{\mathrm{N}i}|=\mu_{\mathrm{S}i}\lambda_i$ ($\mu_{\mathrm{S}i}$ static friction coefficient) is larger than the constraint force $|\boldsymbol{F}_{ci}|=\lambda_{\mathrm{S}i}$ in the tangent plane of contact. We call the difference $(\mu_{\mathrm{S}i}|\boldsymbol{F}_{\mathrm{N}i}|-|\boldsymbol{F}_{ci}|)$ 'friction saturation'. The transition from static to sliding friction takes place for zero friction saturation and non-zero relative acceleration $a_{\mathrm{rel},j}$, which consequently must result in a non-zero velocity $v_{\mathrm{rel},j}$ after the first integration step.

From this we can organize the sequence of events in the following way:

transition sliding to static friction (n_{a} constraints activated),

$$v_{\mathrm{rel},i}(\boldsymbol{q},\dot{\boldsymbol{q}},t)=0 \quad (i\in n_{\mathrm{a}}); \tag{41}$$

static friction state

$$v_{\mathrm{rel},i}(\boldsymbol{q},\dot{\boldsymbol{q}},t)=0, \quad \mu_{\mathrm{S}i}|\boldsymbol{F}_{\mathrm{N}i}|-|\boldsymbol{F}_{ci}|\geqslant 0 \quad (i\in n_{\mathrm{a}}); \tag{42}$$

transition static to sliding friction

$$\mu_{Sj}|\boldsymbol{F}_{\mathrm{N}j}|-|\boldsymbol{F}_{cj}|=0, \quad a_{\mathrm{rel},j}(\boldsymbol{q},\dot{\boldsymbol{q}},t)\neq 0; \tag{43}$$

sliding friction state (see (35))

$$v_{\mathrm{rel},j}(\boldsymbol{q},\dot{\boldsymbol{q}},t)\neq 0, \quad \boldsymbol{F}^{*}_{\mathrm{T}i}=-\boldsymbol{w}_{\mathrm{S}i}\lambda_i\in\mathbb{R}^7. \tag{44}$$

For finding out a beginning transition all indicators must be evaluated and checked for a change of sign. A transition event is going to happen in that contact $k\in 2$, where the transition condition is fulfilled in shortest time, formally:

$$(\Delta t_k)_{GS}=\min_{j\in 2}\{(\Delta t_j)_{GS}\,|\,v_{\mathrm{rel},j}(\boldsymbol{q},\dot{\boldsymbol{q}},t)=0\wedge(\mu_{Sj}|\boldsymbol{F}_{\mathrm{N}j}|-|\boldsymbol{F}_{cj}|)\geqslant 0\}, \tag{45}$$

$$(\Delta t_k)_{SG}=\min_{j\in 2}\{(\Delta t_j)_{SG}\,|\,(\mu_{Sj}|\boldsymbol{F}_{\mathrm{N}j}|-|\boldsymbol{F}_{cj}|)=0\wedge a_{\mathrm{rel},j}(\boldsymbol{q},\dot{\boldsymbol{q}},t)\neq 0\}. \tag{46}$$

The first $(\Delta t_k)_{GS}$ is the time step from some transition event having taken place in some contact to a new transition sliding-static-friction taking place in contact k. The second $(\Delta t_k)_{SG}$ is the shortest time step from a static to a sliding friction mode in contact k. Each transition event generates a new combination of contact constraints. Therefore, the constraint matrices in (38) have to be arranged in a new manner. This property leads to a time-variant topology of the system. Interpolating switching points includes some severe numerical problems with respect to the physical consistency of the solution. Details may be found in the doctoral dissertation of Hajek (1990).

3. Results

3.1. *Comparison with experiments*

In a first step it was necessary to prove the theory by experiments considering the fact that little experience exists about the reality of modelling a sequence of switching points and transitions. Therefore, a test set-up has been established which

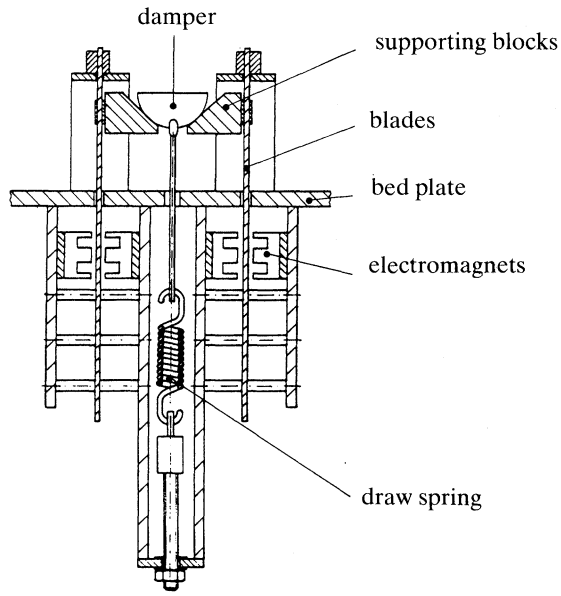

Figure 6. Test set-up for blade damper system (Hajek 1990).

represents an experimental model of a blade damper combination (figure 6). The damper is realized by steel elements of parabolic and circular shape. The supporting surfaces (figure 1) are represented by two steel-blocks and the blades by two bar-like steel plates. The centrifugal force is realized by a draw spring and the excitation by a couple of electromagnets for each blade. The complete set is mounted on a bed plate. Figure 7 gives an idea of excitation and measurement principles.

The excitation is controlled by a frequency generator, a counter and a phase shifter together with two power amplifiers. Position measurements are performed with inductive displacement transducers (S_1–S_6). The spring force F_Z is measured by a strain gauge set-up (DMS). Data were processed by a signal processing unit and in parallel by a digital computer with an appropriate signal processing software.

Let us first consider some typical measurements. Figure 8 shows a phase plot of the blade vibrations as measured with sensor S_5 (see figure 7). It represents a periodic solution with some higher harmonics. The cycle closes after three revolutions. A useful measure for the damper behaviour is given with those excitation force amplitudes $F_{e,\,\mathrm{limit}}$, which start the damper into a stick–slip motion. Before this event we have stiction in both points of contact.

By augmenting F_e step by step we reach $F_{e,\,\mathrm{limit}}$, where at least in one contact point slippage occurs. We call $F_{e,\,\mathrm{limit}}$ the pull-off amplitude. Figures 9 and 10 show the measured influence of the supporting angle γ and the 'centrifugal force' F_Z on this pull-off amplitude.

Globally, the pull-off amplitudes decrease with increasing block angles γ, which means with a more flat supporting plane. This confirms the physical idea that with small angles γ (figure 2) the tendency for stiction increases. With increasing centrifugal forces F_Z the pull-off amplitudes must be augmented, due to the fact that increasing F_Z means increasing normal forces $F_{\mathrm{N}i}$ in the contact points and thus increasing static friction forces.

The pull-off force amplitudes are again used for a comparison of theory and

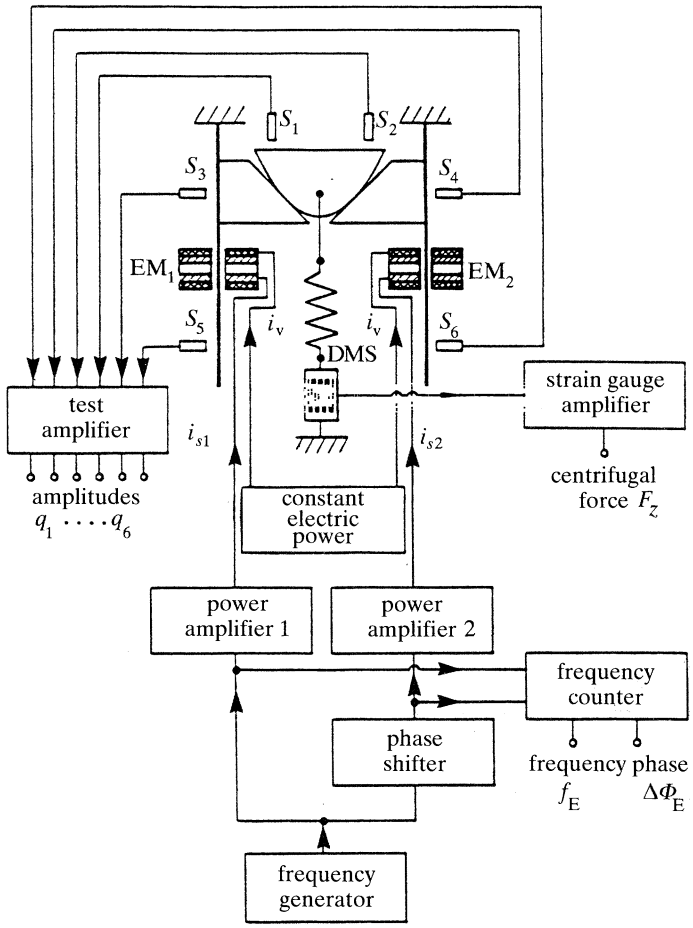

Figure 7. Scheme of set-up for measurements (Hajek 1990). S_1–S_6 are inductive displacement transducers, EM_1 and EM_2 are electromagnets, DMS is the strain gauge bridge, i_r is the magnetic bias and i_{S1}, i_{S2} are control currents.

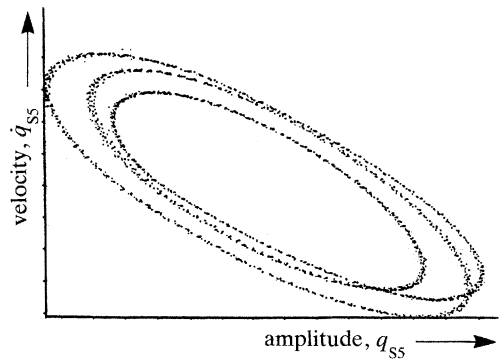

Figure 8. Phase plot of measured blade vibrations.

measurements. Figure 11 gives three examples for different sets of parameters, especially with flat or less flat parabola configurations and with different angles γ. The minimum amplitudes are located at frequencies which correspond to an

Figure 9

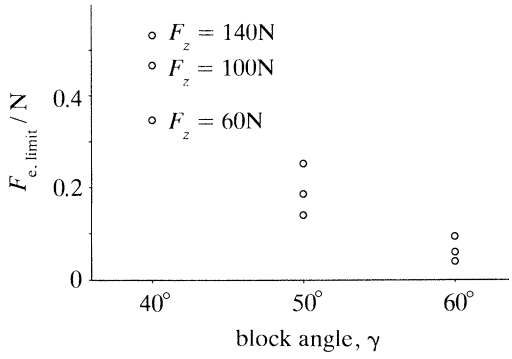

Figure 10

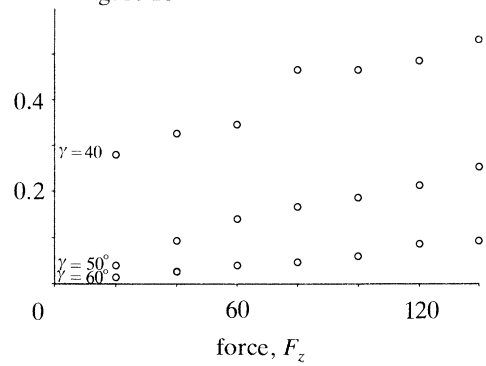

Figure 9. The dependence of pull-off amplitudes on block angle γ and centrifugal force F_Z.
Figure 10. The dependence of pull-off amplitudes on centrifugal force F_z and block angle γ.

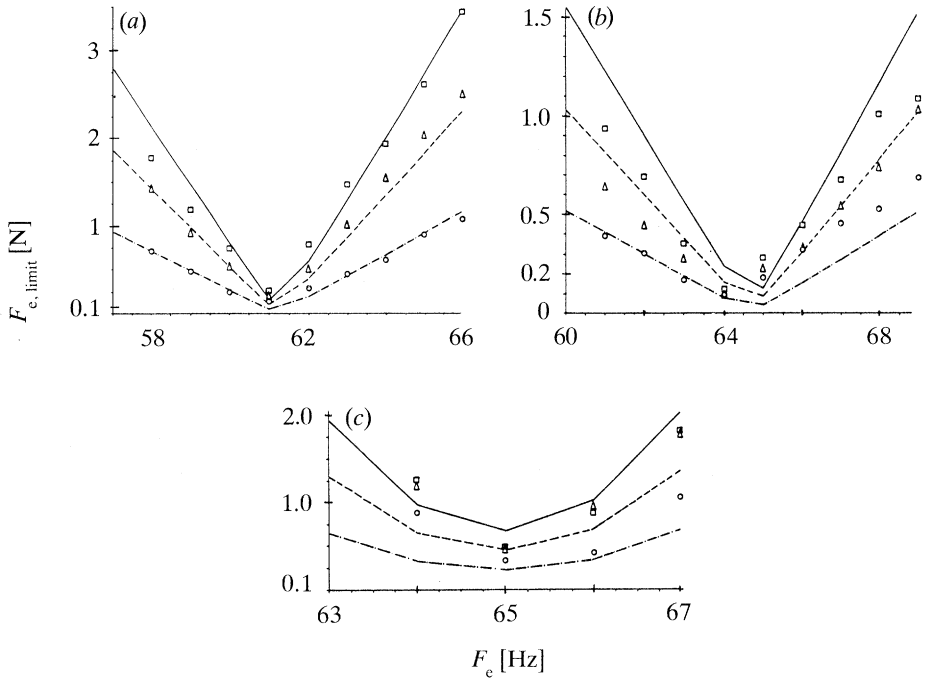

Figure 11. Pull-off amplitudes $F_{e,\,limit}$ against excitation frequency f_e (parameter F_Z) (Hajek 1990). (*a*) Flat parabola, $\gamma = 60°$; (*b*) flat parabola, $\gamma = 50°$; (*c*) medium parabola, $\gamma = 40°$. On each graph for F_z = 60N: ○, measurement; —·—·—, theory. For F_z = 100N: △, measurement; – – –, theory. For F_z = 140N: □, measurement; ——, theory.

eigenfrequency of the blocked system with three degrees of freedom only (case (4)). At such eigenfrequencies the force necessary to induce sliding friction is of course very small.

It should be noted that such eigenfrequencies depend on the configuration, i.e. angle γ, parabola, which can be seen in the three diagrams of figure 11. In the face of a complicated theory the comparisons in figure 11 are excellent and give a certain level of confidence into modelling. This indeed was the basis for a series of parameter

PHILOSOPHICAL TRANSACTIONS OF THE ROYAL SOCIETY A MATHEMATICAL, PHYSICAL & ENGINEERING SCIENCES

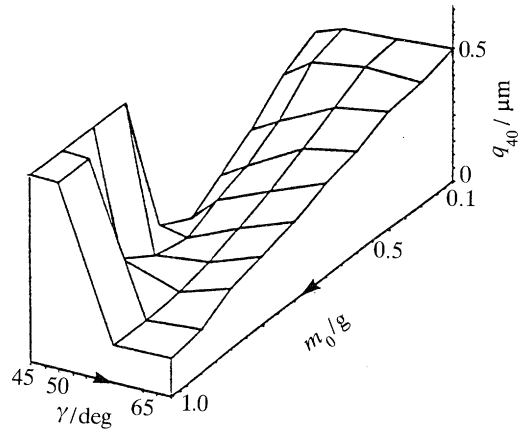

Figure 12. Damper optimization (Hajek 1990).

investigations, where mainly the damper mass, the parabola design (p_1, p_2 in (10)) and the angle γ were considered.

Figure 12 gives a typical example with a significant optimum for a damper mass m_D of about 1 g and an angle γ of about 65°, which represents a flat type of blade base. The coordinate q_{40} is the blade amplitude (figure 2). Parameter optimizations of that type possess considerable value for gas-turbine design.

4. Summary

A damper configuration for gas-turbine blades has been analysed on the basis of a patching method for stick–slip motion. It is assumed that the blade vibrations induce relative motion between damper and blade platforms thus generating dissipation. A planar model for the damper-blade configuration has been developed with two points of contact and a maximum of five degrees of freedom. Depending on the state of motion and due to the time-variant topology of the problem this number can be reduced to three degrees of freedom for stiction in both points of contact. The transitions between static and sliding friction and vice versa are governed by vanishing relative velocities and by the friction saturation, which is the difference between the static friction force and the corresponding constraint force in the same direction. Evaluation of switching points for these transitions is numerically and physically problematic, it must be handled with care. The theory has been compared satisfactorily with experiments performed with the help of a laboratory test set-up. Some parameter optimizations show the design tendencies for good damping behaviour.

References

Beards, C. F. 1985 Damping in structural joints. *Shock Vib. Dig.* **17** (11), 17–20.

Brandl, H. & Hajek, M. 1988 Mechanische Systeme mit Trockenreibung. *Z. angew. Math. Mech.* **64** (4), T59–T61.

Brandl, H., Johanni, R. & Otter, M. 1987 A very efficient algorithm for the simulation of robots and similar multibody systems without inversion of the mass-matrix. In *Proc. IFAC/IFIP/IMACS Int. Symp. on the Theory of Robots*. Wien.

den Hartog, J. P. 1931 Forced vibrations with combined coulomb and viscous friction. *Trans. ASME* **52**, 107–115.

Goodman, L. E. & Klumpp, J. H. 1956 Analysis of slip damping with reference to turbine blade vibration. *J. appl. Mech.* **23**, 421–429.

Griffin, J. H. 1981 An analytical comparison of blade-to-blade and blade-to-ground dampers for use in gas turbine engines. In *Proc. Eighth Canadian Congr. of Applied Mechanics*, pp. 405–406. Moncton.

Guckenheimer, J. & Holmes, P. 1983 *Nonlinear oscillations, dynamical systems and bifurcations of vector fields*. New York, Berlin, Heidelberg, Tokyo: Springer-Verlag.

Hajek, M. 1990 *Reibungsdämpfer für Turbinenschaufeln*. Fortschrittberichte VDI, Reihe 11: Schwingungstechnik, Nr. 128, VDI-Verlag, Düsseldorf.

Hundal, M. S. 1979 Response of a base excited system with coulomb and viscous friction. *J. Sound Vib.* **64**, 371–378.

Jones, D. I. G. & Muszynska, A. 1978 Design of turbine blades for effective slip damping at high rotational speeds. In *Proc. 49th Shock Vib. Symp.*

Jones, D. I. G. & Muszynska, A. 1979 Design of turbine blades for effective slip damping at high rotational speeds. *Shock Vib. Bull.* **49** (2).

Kato, S. 1974 Stick motion of a machine tool slideway. *J. Engng Ind. Trans. ASME*, 557–566.

Klotter, K. 1938 Theorie der Reibungsschwingungsdämpfer. *Ing. Arch.* **9**, 137–162.

Lalanne, M. 1985 Vibration problems in jet engines. *Shock Vib. Dig.* **17** (3), 19–24.

Lötstedt, P. 1981 Coulomb friction in two-dimensional rigid body systems. *Z. angew. Math. Mech.* **61**, 605–615.

Lötstedt, P. 1982 Mechanical systems of rigid bodies subject to unilateral constraints. *SIAM J. appl. Math.* **42**, 281–296.

Lötstedt, P. 1979 A numerical method for the simulation of mechanical systems with unilateral constraints. *Technical Report TRITA-NA-7920*. Sweden: The Royal Institute of Technology.

Magnus, K. 1976 *Schwingungen*. Stuttgart: Teubner Verlag.

Marui, E. & Kato, S. 1984 Forced vibration of a base excited single-degree-of-freedom system with dry friction. *J. Dyn. Sys. Measurem. Contr.* **106**, 280–285.

Moreau, J. J. 1985*a* Dynamique de systemes a liaisons unilaterales aved frottement sec eventuel; essais numeriques. Note Technique 85-1, Lab. de Mecanique Generale des Milieux Continues, Univ. des Sci. et Techniques du Languedoc, Montpellier.

Moreau, J. J. 1985*b* Unilateral problems in structural analysis, kap. standard inelastic shocks and the dynamics of unilateral constraints, pp. 173–221. *CISM courses and lectures*. Wien, New York: Springer-Verlag.

Moreau, J. J. 1988 Nonsmooth mechanics and applications, kap. unilateral contact and dry friction in finite freedom dynamics. *CISM courses and lectures*. Wien, New York: Springer-Verlag.

Panagiotopoulos, P. D. 1985 *Inequality problems in mechanics and applications*. Basel, Boston, Stuttgart: Birkhäuser Verlag.

Pfeiffer, F. 1984 Mechanische Systeme mit unstetigen Übergängen. *Ing. Archiv.* **54**, 232–240.

Pfeiffer, F. 1991 Dynamical systems with time-varying or unsteady structure. *Z. angew. Math. Mech.* **71**, T6–T22.

Ramamurti, V. & Balasubramanian, P. 1984 Analysis of turbomachine blades – a review. *Shock Vib. Dig.* **16** (8), 13–28.

Rao, J. S. 1980 Turbomachine blade vibration. *Shock Vib. Dig.* **12** (2), 19–26.

Reissig, R. 1954 Erzwungene Schwingungen mit zäher und trockener Reibung. *Math. Nachr.* **11**, 345–384.

Reissig, R. 1954 Erzwungene Schwingungen mit zäher und trockener Reibung. *Math. Nachr.* **12**, 283–300.

Schiehlen, W. 1983 Reibungsbehaftete Bindungen in Mehrkörpersystemen. *Ing. Arch.* **53**, 265–273.

Shaw, S. W. 1986 On the dynamic response of a system with dry friction. *J. Sound Vib.* **108**, 305–325.

Sinha, A. & Griffin, J. H. 1983 Friction damping of flutter in gas turbine engine airfoils. *J. Aircraft* **20**, 372–376.

PHILOSOPHICAL TRANSACTIONS OF THE ROYAL SOCIETY A MATHEMATICAL, PHYSICAL & ENGINEERING SCIENCES